

**NUMERICAL STUDY OF SLIP EFFECTS ON UNSTEADY ASYMMETRIC  
BIOCONVECTIVE NANOFLUID FLOW IN A POROUS MICROCHANNEL WITH AN  
EXPANDING/ CONTRACTING UPPER WALL USING BUONGIORNO'S MODEL**

**O. Anwar Bég<sup>1\*</sup>, Md. Faisal Md Basir<sup>2\*</sup>, M.J. Uddin<sup>3</sup> and A. I. Md. Ismail<sup>2</sup>**

<sup>1</sup> *Fluid Mechanics, Biomechanics and Propulsion, Aeronautical and Mechanical Engineering  
Division, Room UG17, Newton Building, University of Salford, M54WT, UK.*

<sup>2</sup> *School of Mathematical Sciences, Universiti Sains Malaysia, 11800, Penang, Malaysia.*

<sup>3</sup> *American International University-Bangladesh, Banani, Dhaka 1213, Bangladesh.*

*\*Corresponding author: Email: O.A.Beg@salford.ac.uk; gortoab@gmail.com*

**ABSTRACT**

In this paper, the unsteady fully developed forced convective flow of viscous incompressible biofluid that contains both nanoparticles and gyrotactic microorganisms in a horizontal micro-channel is studied. Buongiorno's model is employed. The upper channel wall is either expanding or contracting and permeable and the lower wall is static and impermeable. The plate separation is therefore a function of time. Velocity, temperature, nano-particle species (mass) and motile micro-organism slip effects are taken into account at the upper wall. By using the appropriate similarity transformation for the velocity, temperature, nanoparticle volume fraction and motile microorganism density, the governing partial differential conservation equations are reduced to a set of similarity ordinary differential equations. These equations under prescribed boundary conditions are solved numerically using the Runge-Kutta-Fehlberg fourth-fifth order numerical quadrature in the MAPLE symbolic software. Excellent agreement between the present computations and solutions available in the literature (for special cases) is achieved. The key thermofluid parameters emerging are identified as Reynolds number, wall expansion ratio, Prandtl number, Brownian motion parameter, thermophoresis parameter, Lewis number, bioconvection Lewis number and bioconvection Péclet number. The influence of all these parameters on flow velocity, temperature, nano-particle volume fraction (concentration) and motile micro-organism density function is elaborated. Furthermore graphical solutions are included for skin friction, wall heat transfer rate, nano-particle mass transfer rate and micro-organism transfer rate. Increasing expansion ratio is observed to enhance temperatures and motile micro-organism density. Both nanoparticle volume fraction and microorganism increases with an increase in momentum slip. The dimensionless temperature and microorganism increases as wall expansion increases. Applications of the study arise in advanced nanomechanical bioconvection energy conversion devices, bio-nano-coolant deployment systems etc.

**Keywords:** *Multiple slip, bioconvection, nanofluids, unsteady flow; micro-channel; porous wall; gyrotactic microorganisms; expanding/contracting upper wall; numerical.*

## NOMENCLATURE

$a$	length of channel ( $m$ )
$\dot{a}$	time-dependent rate $\left(\frac{m}{s}\right)$
$a_1$	velocity slip parameter, $\left(a_1 = \frac{S_1 \nu}{a}\right)$ (-)
$A$	injection coefficient $\left(\frac{m}{s}\right)$
$\tilde{b}$	chemotaxis constant ( $m$ )
$b_1$	thermal slip parameter, $\left(b_1 = \frac{D_1}{a}\right)$ (-)
$C$	nano-particles volume fraction (-)
$C_0$	reference nano-particle volume fraction (-)
$C_1$	nano-particle volume fraction on lower wall (-)
$C_2$	nano-particle volume fraction on lower wall (-)
$c_1$	mass slip parameter, $\left(c_1 = \frac{E_1}{a}\right)$ (-)
$c_p$	specific heat at constant pressure $\left(\frac{J}{kgK}\right)$
$D_B$	Brownian diffusion coefficient $\left(\frac{m^2}{s}\right)$
$D_n$	variable micro-organism diffusion coefficient $\left(\frac{m^2}{s}\right)$
$D_T$	thermophoretic diffusion coefficient $\left(\frac{m^2}{s}\right)$
$D_1$	thermal slip factor ( $m$ )
$d_1$	micro-organism slip parameter, $\left(d_1 = \frac{F_1}{a}\right)$ (-)
$E_1$	mass slip factor ( $m$ )
$F_1$	micro-organism slip factor ( $m$ )
$f(\eta)$	dimensionless stream function (-)

$\vec{j}$	vector flux of micro-organisms $\left(\frac{kg}{m^2 s}\right)$
$k$	thermal conductivity $\left(\frac{W}{mK}\right)$
$Nb$	Brownian motion parameter $\left(Nb = \frac{\tau D_B (C_2 - C_0)}{\alpha_0}\right) (-)$
$Nt$	thermophoresis parameter $\left(Nt = \frac{\tau D_T (T_2 - T_0)}{\alpha_0 T_0}\right) (-)$
$N$	number of motile micro-organisms $(-)$
$N_1$	lower wall motile micro-organisms $(-)$
$N_2$	upper wall motile micro-organisms $(-)$
$p$	pressure $\left(\frac{Newton}{m^2}\right) (-)$
$Pe$	bioconvection Péclet number $\left(Pe = \frac{\tilde{b} W_c}{D_n}\right) (-)$
$Pr$	Prandtl number $\left(Pr = \frac{\nu}{\alpha_0}\right) (-)$
$Re$	Reynolds number $\left(\frac{av_w}{\nu}\right) (-)$
$S_1$	velocity slip factor $\left(\frac{s}{m}\right)$
$Lb$	bioconvection Lewis number $\left(Sb = \frac{\alpha_0}{D_n}\right) (-)$
$Le$	Lewis number $\left(Le = \frac{\alpha_0}{D_B}\right) (-)$
$\bar{t}$	dimensional time $(s)$
$T$	nanofluid temperature $(K)$
$T_0$	reference temperature $(K)$
$T_1$	temperature on lower wall $(K)$
$T_2$	temperature on upper wall $(K)$
$\bar{u}$	velocity components along the $\bar{x}$ - axis $\left(\frac{m}{s}\right)$
$\vec{v}$	velocity vector $\left(\frac{m}{s}\right)$
$\hat{v}$	average swimming velocity vector of micro-organism $\left(\frac{m^2}{s}\right)$

$\bar{v}$	velocity components along the $\bar{y}$ – axis $\left(\frac{m}{s}\right)$
$\bar{v}_w$	dimensional inflow/outflow velocity $\left(\frac{m}{s}\right)$
$W_c$	maximum cell swimming speed $\left(\frac{m}{s}\right)$
$\bar{x}$	dimensional coordinate along the surface $(m)$
$\bar{y}$	coordinate normal to the surface $(m)$

### Greek letters

$\alpha_0$	effective thermal diffusivity $\left(\frac{m^2}{s}\right)$
$\alpha$	wall expansion ratio $\left(\frac{a\dot{a}}{\nu}\right)$
$\eta$	independent similarity variable $(-)$
$\theta(\eta)$	dimensionless temperature $(-)$
$\theta_1$	constant $(-)$
$\nu$	kinematic viscosity $\left(\frac{m^2}{s}\right)$
$\rho$	fluid density $\left(\frac{kg}{m^3}\right)$
$(\rho c)_f$	volumetric heat capacity of the fluid $\left(\frac{J}{m^3 K}\right)$
$(\rho c)_p$	volumetric heat capacity of the nanoparticle material $\left(\frac{J}{m^3 K}\right)$
$\tau$	ratio of the effective heat capacity of the nanoparticle material to the fluid heat capacity $\left(\frac{(\rho c)_p}{(\rho c)_f}\right)(-)$
$\phi(\eta)$	dimensionless nanoparticles volume fraction $(-)$
$\phi_1$	constant $(-)$
$\chi(\eta)$	dimensionless number of motile micro-organisms $(-)$
$\chi_1$	constant $(-)$

### Subscripts

$( )'$	ordinary differentiation with respect to $\eta$
--------	---

$( )_0$	condition at reference
$( )_1$	condition at lower wall
$( )_2$	condition at upper wall

## 1. INTRODUCTION

The recent progress in scaling down devices in medical engineering requires a more elegant and refined understanding of fluid dynamic, heat and mass transfer phenomena at small scales. Responding to this demand, numerous scientists and engineers are actively studying methods for enhancing heat, mass and momentum transfer strategies at the micro-dimension scale. Usually channels with hydraulic diameter below 1 mm are categorized as *micro-channels*. They arise in diverse areas of health technology including efficient micro-sized cooling systems for biomedical processing systems, bio-electronic devices, lab-on-a-chip biological designs, bio-astronautics, cell sorting, immunoassays, DNA sampling etc [1]. One aspect distinguishing micro/nanoscale gas flows from their macroscale counterparts is that the *wall slip* effect usually becomes so vital at micro/nanoscales that its negligence may lead to predictions deviating unacceptably from physical reality. Employing the Navier–Stokes equations in conjunction with adequate slip velocity boundary conditions that properly incorporate gas molecule and wall interaction kinetics, has been demonstrated to be a robust methodology for providing accurate results for micro/nanoscale gas flows as described by Wu [2]. Numerous studies have revealed the important influence of slip on near-wall flow characteristics.

The internal flow through a porous channel with extending/contracting walls has some important applications in biophysical flows such as blood flow and artificial dialysis, air and blood circulation in the respiratory system. Further applications include filtration in tissue, oxygen diffusion in capillaries, cosmetics materials manufacture, the mechanics of the cochlea in the human ear, pulsating diaphragms and cerebral hydrodynamics [3, 4]. A significant number of investigations have been communicated recently on internal fluid dynamics of porous channels under different wall conditions and for various transport phenomena. Adesanya [5] examined natural convective flow of heat generating fluid through a permeable channel with anisotropic slip. A seminal early analysis was presented by Uchida and Aoki [6] concerning viscous flow through a tube with a contracting cross section. Later Bujurke [7] further considered the Uchida-Aoki model both analytically with series expansions and numerically. Goto and Uchida [8] presented an unsteady laminar flow model for incompressible fluid through a permeable pipe. Other recent studies focused on fluid

mechanics in a porous channel with a contracting and/or expanding wall include the works by Hatami *et al.* [9], Boutros *et al.* [10], Xinhui *et al.* [11], Si *et al.* [12], Ahmed *et al.* [13] and Darvishi *et al.* [14]. These articles have considered many multi-physical effects including non-Newtonian fluids, magnetohydrodynamics, chemical reaction and heat and mass transfer.

Nanofluids also constitute a significant development in thermofluid dynamics in recent years. The term nanofluid was popularized by Choi [15]. A *nanofluid* is characterized as the suspension synthesized via scattering of nano-sized particles in a base fluid. With the rapid develops in nano-manufacturing, many low-cost combinations of liquid/particle are now obtainable. These include particles of metals such aluminum, copper, gold, iron and titanium or their oxides. The base fluids used are usually water, ethylene glycol, toluene and oil. A key feature of nanofluids is their demonstrated ability to improve the efficiency of heat transfer equipment as documented by Eastman *et al.* [16]. Khairul *et al.* [17] reported on experimental results concerning the impressive thermal properties of the nanofluids. The acceleration in deployment of nanofluids has required both extensive laboratory and field testing and also theoretical and computational simulations. The fundamental idea of nanofluids is to combine the two substances to form a heat transfer medium that behaves like a fluid, but has the high thermal conductivity characteristics of a metal. Nanofluids have therefore been deployed in a wide spectrum of technological applications including microelectronics, solar cells, pharmaceutical processes, hybrid-powered engines, vehicle thermal management, refrigeration/chiller systems, heat exchangers, nuclear reactor coolants, lubricants, space technology, combustion devices and rocket propellants, as elaborated by Bég and Tripathi [18]. Extensive reviews and analyses of nanofluids have been reported by many researchers – see for example Kakaç and Pramuanjaroenkij [19], Hamad and Ferdows [20].

A substantial thrust in modern fluid mechanics has been *biological transport*. A subset of such flows is *bioconvection*. Bioconvection can be defined as pattern formation in suspensions of microorganisms, such as bacteria and algae, due to up-swimming of the microorganisms towards a specific taxis e.g. light, gravity, chemicals, magnetic fields, oxygen. Detailed elaboration is given in Pedley *et al.* [21]. It results from an unstable density stratification induced by upswimming microorganisms which occurs when the microorganisms (heavier than water) accumulate in the upper regions of the fluid, manifesting in a special type of hydrodynamic instability which are observable as bioconvection plumes, as discussed by Uddin *et al.* [22]. A refinement in bioconvection is

achieved by the careful suspension of microorganisms in *nanofluids* which serves to enhance thermal conductivity as well as stability of the resulting bio-nanofluid. Raees *et al.* [23] studied computationally the forced/free convection in buoyancy-driven nano-liquid film flow containing gyrotactic microorganisms using both a passively and actively controlled nanofluid with a finite difference technique. Raees *et al.* [24] simulated numerically the unsteady squeezing flow and heat transfer through a channel in a nanofluid containing microorganisms with wall expansion and contraction effects. Basir *et al.* [25] investigated transient multi-slip nanofluid bioconvection from an extending cylindrical body and considered the effects of hydrodynamic, thermal and micro-organism slip.

Motivated by further refining physico-mathematical modelling of channel bioconvection nanofluid flows, in the present work, we extend the analysis of Xinhui *et al.* [11] to obtain solutions of the flow, heat, nano-particle and micro-organism diffusion in unsteady bioconvective nanofluid flow in a porous channel with an expanding and contracting wall. Here we considered four slip mechanisms i.e. velocity, thermal, mass (nano-particle species) and micro-organism slip at the *upper wall* of a two-dimensional channel. The channel plates are parallel, the upper plate being porous and the lower plate being impermeable. Validation of the solution obtained is achieved with an excellent agreement.

## 2. MATHEMATICAL MODEL

Consider a two-dimensional unsteady laminar forced bioconvective slip flow of nanofluid in a horizontal semi-infinite channel with the distance  $\bar{a}(\bar{t})$  between two walls (see **Fig. 1**). The upper channel wall has nanofluid injected at velocity,  $\bar{v}_w$ , and is expanding *or* contracting uniformly at a time-dependent rate,  $\frac{\partial \bar{a}}{\partial t}$ . The plate separation is therefore a function of time and equals  $\bar{a}(\bar{t})$ . The lower channel wall is a *static impermeable* surface. The coordinate system is selected such that the  $\bar{x}$  – axis is along the lower plate and the  $\bar{y}$  – axis is normal to the plate.  $\bar{u}$  and  $\bar{v}$  denote the velocity components in the  $\bar{x}$  and  $\bar{y}$  directions, respectively.  $T, C, N$  are the temperature of the fluid, the nanoparticle volume fraction and density of motile micro-organisms, respectively. The temperatures are assumed to be constant on the lower and upper walls and are denoted, respectively by  $T_1$  and  $T_2$ . In addition to this, the nanoparticle volume fraction on the upper wall is  $C_2$  and that on the

lower wall is  $C_1$ . The density of motile microorganisms on the upper wall is prescribed as  $N_2$  and on the lower wall as  $N_1$ .

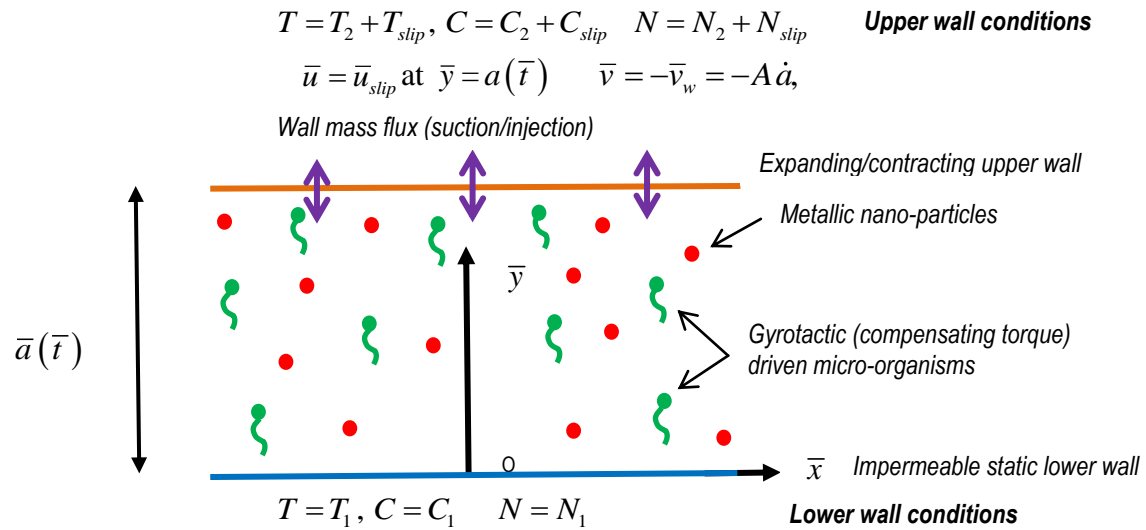


**Figure 1:** Physical configuration for bioconvection nanofluid slip channel flow with an expanding or contracting wall (model for adaptive microbial nanofluid fuel cell)

Here the base fluid is taken as water and nano-particles are suspended in the base fluid. The resulting nanofluid is assumed to be stable and does not permit agglomeration in the fluid, thereby allowing the micro-organisms to be alive [24]. Also the direction of microorganism's swimming is *independent* of nanoparticles [25]. Under these assumptions we employ the Buongiorno nanofluid model [26] which emphasizes Brownian motion and thermophoresis as the principal mechanisms for nano-particle thermal enhancement. This model generally assumes that the nanofluid is dilute and contains a homogenous suspension of equally-sized, nano-particles in thermal equilibrium. It infers that thermophoresis and Brownian motion effects dominate over other nanoscale effects such as ballistic collisions, micro-convection patterns etc. The Buongiorno model has been proven to widely applicable in nanoscale transport phenomena and extensive investigations have been reported. These include Malvandi *et al.* [27] for buoyancy-driven pumping, Xu *et al.* [28] for mixed convection, Sheremet *et al.* [29] for nanofluid flows in porous media enclosures, Akbar *et al.* [30] for electro-conductive nanofluid extrusion, Uddin *et al.* [31] for high temperature radiative processing of aerospace nanomaterials and also very recently by Uddin *et al.* [32] for anisotropic slip stagnation nanofluid gyrotactic bioconvection flows. Buongiorno's model



was originally adapted for laminar boundary layers by Kuznetsov and Nield [33]. Using this model, the governing partial differential equations of *mass, momentum, thermal energy, nano-particle concentration and micro-organism density conservation* emerge in the following forms:

$$\nabla \cdot \vec{\bar{v}} = 0, \quad (1)$$

$$\frac{\partial \vec{\bar{v}}}{\partial t} + (\vec{\bar{v}} \cdot \nabla) \vec{\bar{v}} = -\frac{1}{\rho} \nabla p + \nu \nabla^2 \vec{\bar{v}}, \quad (2)$$

$$\frac{\partial T}{\partial t} + (\vec{\bar{v}} \cdot \nabla) T = \alpha_0 \nabla^2 T + \tau \left[ D_B \nabla T \cdot \nabla C + \left( \frac{D_T}{T_0} \right) \nabla T \cdot \nabla T \right], \quad (3)$$

$$\frac{\partial C}{\partial t} + (\vec{\bar{v}} \cdot \nabla) C = D_B \nabla^2 C + \tau \left[ \left( \frac{D_T}{T_0} \right) \nabla^2 T \right], \quad (4)$$

$$\frac{\partial n}{\partial t} + \nabla \cdot \vec{j} = 0 \quad (5)$$

Here  $\vec{\bar{v}} = (\bar{u}, \bar{v})$  are the velocity components along and perpendicular to the wall,  $p$  is the

pressure,  $\tau = \frac{(\rho c)_p}{(\rho c)_f}$  is the ratio of nano-particle heat capacity and the base fluid heat

capacity,  $\alpha_0 = \frac{k}{(\rho c)_f}$  is the thermal diffusivity of the fluid,  $\rho$  is the density of the base fluid,

$\nu$  is the kinematic viscosity,  $D_B$  is the Brownian diffusion coefficient and  $D_T$  is the thermophoresis diffusion coefficient,  $T_0$  is the reference temperature. Furthermore,  $\vec{j}$  which denotes the flux of microorganisms can be written as:

$$\vec{j} = N \vec{\bar{v}} + N \hat{\vec{v}} - D_n \nabla N \quad (6)$$

Also  $\hat{\vec{v}} = \left( \frac{\tilde{b} W_c}{C_2 - C_0} \right) \nabla C$  is the average swimming velocity vector of micro-organisms in

nanofluids,  $D_n$  designates the species diffusivity of micro-organisms,  $\tilde{b}$  denotes the chemotaxis constant,  $W_c$  signifies the maximum cell swimming speed,  $C_0$  is the reference

concentration and  $\nabla C = \frac{\partial C}{\partial y}$ . For the two-dimensional case, Eqns. (2)–(5) can be written as:

$$\frac{\partial \bar{u}}{\partial x} + \frac{\partial \bar{v}}{\partial y} = 0, \quad (7)$$

$$\frac{\partial \bar{u}}{\partial \bar{t}} + \bar{u} \frac{\partial \bar{u}}{\partial \bar{x}} + \bar{v} \frac{\partial \bar{u}}{\partial \bar{y}} = -\frac{1}{\rho} \frac{\partial p}{\partial \bar{x}} + \nu \left( \frac{\partial^2 \bar{u}}{\partial \bar{x}^2} + \frac{\partial^2 \bar{u}}{\partial \bar{y}^2} \right), \quad (8)$$

$$\frac{\partial \bar{v}}{\partial \bar{t}} + \bar{u} \frac{\partial \bar{v}}{\partial \bar{x}} + \bar{v} \frac{\partial \bar{v}}{\partial \bar{y}} = -\frac{1}{\rho} \frac{\partial p}{\partial \bar{y}} + \nu \left( \frac{\partial^2 \bar{v}}{\partial \bar{x}^2} + \frac{\partial^2 \bar{v}}{\partial \bar{y}^2} \right), \quad (9)$$

$$\begin{aligned} \frac{\partial T}{\partial \bar{t}} + \bar{u} \frac{\partial T}{\partial \bar{x}} + \bar{v} \frac{\partial T}{\partial \bar{y}} &= \alpha_0 \left( \frac{\partial^2 T}{\partial \bar{x}^2} + \frac{\partial^2 T}{\partial \bar{y}^2} \right) \\ &+ \tau \left[ D_B \left( \frac{\partial T}{\partial \bar{x}} \frac{\partial C}{\partial \bar{x}} + \frac{\partial T}{\partial \bar{y}} \frac{\partial C}{\partial \bar{y}} \right) + \frac{D_T}{T_0} \left[ \left( \frac{\partial T}{\partial \bar{x}} \right)^2 + \left( \frac{\partial T}{\partial \bar{y}} \right)^2 \right] \right], \end{aligned} \quad (10)$$

$$\frac{\partial C}{\partial \bar{t}} + \bar{u} \frac{\partial C}{\partial \bar{x}} + \bar{v} \frac{\partial C}{\partial \bar{y}} = D_B \left( \frac{\partial^2 C}{\partial \bar{x}^2} + \frac{\partial^2 C}{\partial \bar{y}^2} \right) + \frac{D_T}{T_0} \left( \frac{\partial^2 C}{\partial \bar{x}^2} + \frac{\partial^2 C}{\partial \bar{y}^2} \right), \quad (11)$$

$$\frac{\partial N}{\partial \bar{t}} + \bar{u} \frac{\partial N}{\partial \bar{x}} + \bar{v} \frac{\partial N}{\partial \bar{y}} + \frac{\tilde{b}W_c}{C_2 - C_0} \left[ \frac{\partial}{\partial \bar{x}} \left( N \frac{\partial C}{\partial \bar{x}} \right) + \frac{\partial}{\partial \bar{y}} \left( N \frac{\partial C}{\partial \bar{y}} \right) \right] = D_n \left( \frac{\partial^2 N}{\partial \bar{x}^2} + \frac{\partial^2 N}{\partial \bar{y}^2} \right). \quad (12)$$

The relevant boundary conditions are following Dauenhauer and Majdalani [34], Cao *et al.* [35] and Raza *et al.* [36]:

$$\begin{aligned} \bar{u} &= \bar{u}_{slip}, \quad \bar{v} = -\bar{v}_w = -A\dot{\bar{a}}(\bar{t}), \\ T &= T_2 + T_{slip}, \quad C = C_2 + C_{slip}, \quad N = N_2 + N_{slip} && \text{at } \bar{y} = \bar{a}(\bar{t}) \\ \bar{u} &= 0, \quad \bar{v} = 0, \quad T = T_1, \quad C = C_1, \quad N = N_1 && \text{at } \bar{y} = 0 \end{aligned} \quad (13)$$

where  $\bar{u}_{slip} = S_1 \nu \frac{\partial \bar{u}}{\partial \bar{y}}$  is the linear slip velocity,  $S_1$  is the velocity slip factor,  $T_{slip} = D_1 \frac{\partial T}{\partial \bar{y}}$  is

the thermal slip,  $D_1$  is the thermal slip factor,  $C_{slip} = E_1 \frac{\partial C}{\partial \bar{y}}$  is the mass (nano-particle) slip,

$E_1$  is the mass (nano-particle) slip factor,  $N_{slip} = F_1 \frac{\partial N}{\partial \bar{y}}$  is the micro-organism slip and  $F_1$  is

the micro-organism slip factor.  $A = \bar{v}_w / \dot{\bar{a}}(\bar{t})$  is the coefficient of the injection which is a measure of permeability of the wall [34]. Defining the following similarity transformations [11]:

$$\eta = \frac{\bar{y}}{\bar{a}(\bar{t})}, \quad \bar{u} = -\frac{\nu}{\bar{a}^2(\bar{t})} \bar{x} F'(\eta, \bar{t}), \quad \bar{v} = \frac{-\nu}{\bar{a}(\bar{t})} F(\eta, \bar{t}),$$

$$\theta(\eta) = \frac{T - T_0}{T_2 - T_0}, \quad \phi(\eta) = \frac{C - C_0}{C_2 - C_0}, \quad \chi(\eta) = \frac{N}{N_2}.$$
(14)

By substituting Eqns. (14) into Eqns. (7) – (12) together with boundary conditions (13) and eliminating the pressure gradient terms from the momentum equations (8) and (9), the resulting system of similarity differential equations with respect to both time and space can be obtained following transformation [6], [11]: as follows:

$$f^{iv} + \text{Re}(ff''' - f'f'') + \alpha(\eta f''' + 3f'') = 0 \quad (15)$$

$$\theta'' + \text{Pr Re } f \theta' + \text{Nb } \phi' \theta' + \text{Nt } \theta'^2 + \text{Pr } \alpha \eta \theta' = 0 \quad (16)$$

$$\phi'' + \text{Pr Le Re } f \phi' + \frac{\text{Nt}}{\text{Nb}} \theta'' + \text{Pr Le } \alpha \eta \phi' = 0 \quad (17)$$

$$\chi'' - \text{Pe} (\phi' \chi' + \chi \phi'') + \text{Lb Pr Re } f \chi' + \text{Lb Pr } \alpha \eta \chi' = 0 \quad (18)$$

where  $f = \frac{F}{\text{Re}}$ ,  $\text{Re} = \frac{av_w}{\nu}$  is the permeation Reynolds number,  $\alpha = \frac{a \dot{a}}{\nu}$  is the wall expansion

ratio,  $\text{Pr} = \frac{\nu}{\alpha_0}$  is the Prandtl number,  $\text{Nb} = \frac{\tau D_B (C_2 - C_0)}{\alpha_0}$  is the Brownian motion

parameter,  $\text{Nt} = \frac{\tau D_T (T_2 - T_0)}{\alpha_0 T_0}$  is the thermophoresis parameter,  $\text{Le} = \frac{\alpha_0}{D_B}$  is the Lewis

number,  $\text{Lb} = \frac{\alpha_0}{D_n}$  is the bioconvection Lewis number and  $\text{Pe} = \frac{\tilde{b} W_c}{D_n}$  is the bioconvection

Péclet number. Note that  $\alpha > 0$  corresponds to an expanding upper wall and  $\alpha < 0$  corresponds to a contracting upper wall. For  $\alpha = 0$  the upper wall is *static i.e. the channel plate separation is fixed*.

The corresponding boundary conditions are:

$$f(0) = 0, \quad f'(0) = 0, \quad \theta(0) = \theta_1, \quad \phi(0) = \phi_1, \quad \chi(0) = \chi_1,$$
(19)

$$f(1) = 1, \quad f'(1) = a_1 f''(1), \quad \theta(1) = 1 + b_1 \theta'(1), \quad \phi(1) = 1 + c_1 \phi'(1), \quad \chi(1) = 1 + d_1 \chi'(1)$$

Where  $a_1 = \frac{S_1 \nu}{a}$  is the velocity slip parameter,  $b_1 = \frac{D_1}{a}$  is the thermal slip parameter,  $c_1 = \frac{E_1}{a}$  is the mass (nano-particle) slip parameter,  $d_1 = \frac{F_1}{a}$  is the microorganism slip parameter, and  $\theta_1 = \frac{T_1 - T_0}{T_2 - T_0}$ ,  $\phi_1 = \frac{C_1 - C_0}{C_2 - C_0}$ ,  $\chi_1 = \frac{N_1}{N_2}$  are constants. In the present work we confine attention to positive permeation Reynolds number which physically corresponds to injection at the upper wall i.e. suction (*negative* permeation Reynolds number is *not* considered since it is not relevant to coolant designs). The model developed herein considers *viscous, incompressible, biological fluid suspensions*. Many such fluids exist including water-based liquids containing bacterial (Bacillus, Chlamydomonas, Volvox, and Tetrahymena), algal or zooplankton suspensions, as elaborated by Pedley and Kessler [37]. The presence of *nano-particles* does not alter the incompressibility or biological nature of such suspensions as the nano-particles do not interact with the motile (i.e. self-propelled) micro-organisms. They are separate “species”. The micro-organisms possess mean diameters which range from 1 to 200 micro-metres and are therefore significantly larger than nano-particle dimensions. These micro-organisms, which are considered to be *gyrotactic* in the present study, possess slightly greater densities than the water base fluid e.g. several percent for algae and no more than 10 percent for bacteria e.g. B. subtilis. Excellent details are provided by Hart & Edwards [38].

### 3. PHYSICAL QUANTITIES FOR MEDICAL ENGINEERING DESIGN

The quantities of practical interest in this study are the Nusselt number  $Nu_{\bar{x}}$ , Sherwood number  $Sh_{\bar{x}}$ , and the density number of motile micro-organisms  $Nn_{\bar{x}}$ , which are defined, respectively as:

$$Nu_{\bar{x}} = \frac{-\bar{a}(\bar{t})q_w}{k(T_2 - T_0)}, \quad Sh_{\bar{x}} = \frac{-\bar{a}(\bar{t})q_m}{D_B(C_2 - C_0)}, \quad Nn_{\bar{x}} = \frac{-\bar{a}(\bar{t})q_n}{D_n N_2}. \quad (20)$$

where  $q_w$ ,  $q_m$  and  $q_n$  represent the surface heat flux, surface mass flux and the surface motile microorganism flux, respectively and are defined by:

$$q_w = -k \left( \frac{\partial T}{\partial \bar{y}} \right)_{\bar{y}=\bar{a}(\bar{t})}, \quad q_m = -D_B \left( \frac{\partial C}{\partial \bar{y}} \right)_{\bar{y}=\bar{a}(\bar{t})}, \quad q_n = -D_n \left( \frac{\partial N}{\partial \bar{y}} \right)_{\bar{y}=\bar{a}(\bar{t})}. \quad (21)$$

Substituting Eqs. (14), (21) into (20), the following expressions are obtained:

$$-\theta'(1) = Nu_{\bar{x}}, \quad -\phi'(1) = Sh_{\bar{x}}, \quad -\chi'(1) = Nn_{\bar{x}}. \quad (22)$$

#### 4. NUMERICAL SOLUTION AND VALIDATION

The two point boundary problem defined by Eqns. (15) – (18) under boundary conditions (19) is strongly nonlinear. A computational method is therefore adopted, namely the Runge-Kutta-Fehlberg fourth-fifth order shooting method available in the Maple software via built-in functions. This method has been successfully used by many researchers in order to solve complex higher order, nonlinear ordinary differential equations (ODEs). The details of the algorithm are lucidly documented in Uddin *et al.* [39], Bég *et al.* [40] and Bég and Makinde [41] and are therefore not repeated here. Validation of the general model developed is not possible with published solutions from the literature and therefore we employ a second order accurate finite difference algorithm known as Nakamura's method to validate the general Maple solutions. The Nakamura tridiagonal method [42] generally achieves fast convergence for nonlinear viscous flows which may be described by either parabolic (boundary layer) or elliptic (Navier-Stokes) equations. **The coupled 10<sup>th</sup>** order system of nonlinear, multi-degree, ordinary differential equations defined by (15)–(18) with boundary conditions (19) is solved using the NANONAK code in double precision arithmetic in Fortran 90, as elaborated by Bég [43]. Computations are performed on an SGI Octane Desk workstation with dual processors and take seconds for compilation. As with other difference schemes, a reduction in the higher order differential equations, is also fundamental to Nakamura's method. The method has been employed successfully to simulate many sophisticated nonlinear transport phenomena problems e.g. magnetized bio-rheological coating flows (Bég *et al.* [44]). Earlier it has been employed in viscoelastic Falkner-Skan flows (Bég *et al.* [45] and rotating micropolar convection flows (Gorla and Nakamura [46]). Intrinsic to this method is the discretization of the flow regime using an equi-spaced finite difference mesh in the transformed coordinate ( $\eta$ ). The partial derivatives for  $f$ ,  $\theta$ ,  $\phi$  and  $\chi$  with respect to  $\eta$  are evaluated by central difference approximations. An iteration loop based on the *method of successive substitution* is utilized to advance the solution i.e. march along. The finite difference discretized equations are solved in a step-by-step fashion on the  $\eta$ -domain. For the energy, nano-particle species and motile micro-organism density conservation Eqns. (16) - (18) which are *second order* multi-degree ordinary differential equations, only a *direct substitution* is needed. However a reduction is required for the *fourth order* momentum Eqn. (25). We apply the following substitutions:

$$P = f''' \quad (23)$$

$$Q = \theta \quad (24)$$

$$R = \phi \quad (25)$$

$$S = \chi \quad (26)$$

The ODEs (15)-(18) then retract to:

***Nakamura momentum equation:***

$$A_1 P'' + B_1 P' + C_1 P = T_1 \quad (27)$$

***Nakamura energy equation:***

$$A_2 Q'' + B_2 Q' + C_2 Q = T_2 \quad (28)$$

***Nakamura nano-particle species equation:***

$$A_3 R'' + B_3 R' + C_3 R = T_3 \quad (29)$$

***Nakamura motile micro-organism density number equation:***

$$A_4 S'' + B_4 S' + C_4 S = T_4 \quad (30)$$

Here  $A_i=1,2,3,4$ ,  $B_i=1,2,3,4$ ,  $C_i=1,2,3,4$  are the Nakamura matrix coefficients,  $T_i=1,2,3,4$  are the Nakamura source terms containing a mixture of variables and derivatives associated with the respective lead variable ( $P$ ,  $Q$ ,  $R$ ,  $S$ ). The Nakamura Eqns. (27)–(30) are transformed to finite difference equations and these are orchestrated to form a tridiagonal system which due to the high nonlinearity of the numerous coupled, multi-degree terms in the momentum, energy, nano-particle species and motile micro-organism density conservation equations, is solved *iteratively*. Householder's technique is ideal for this iteration. The boundary conditions (19) are also easily transformed. Further details of the **NTM** approach are provided in the comprehensive treatise of Nakamura [47]. Applications in non-Newtonian magnetic channel flows are documented in the review by Bég [48]. Comparisons are documented in **Tables 1-4** for heat transfer rate and nano-particle mass transfer rate at the upper wall ( $\eta=1$ ) i.e.  $-\left| \theta'(1) \right|$  and  $-\left| \phi'(1) \right|$ , respectively. Generally very close correlation is obtained over a range of  $\alpha$  (*contracting, expanding and stationary upper wall cases*),  $b_1$  and  $c_1$  values. Confidence in the Maple RK45 numerical solutions is therefore justifiably high.

$b_1$	$-\left \theta'(1)\right $	$-\left \theta'(1)\right $	$-\left \theta'(1)\right $	$-\left \theta'(1)\right $	$-\left \theta'(1)\right $	$-\left \theta'(1)\right $
	Maple	Nakamura	Maple	Nakamura	Maple	Nakamura
	$\alpha=-0.5$	$\alpha=-0.5$	$\alpha=0$	$\alpha=0$	$\alpha=+0.5$	$\alpha=+0.5$
0.25	0.43851662	0.43851788	0.10479830	0.10479828	0.02415781	0.02415742
0.50	0.55356648	0.55356475	0.11035680	0.11035704	0.02444230	0.02444204
0.75	0.74039460	0.74039503	0.11650804	0.11650796	0.02473331	0.02473307
1.00	1.06979037	1.06979217	0.12334615	0.12334589	0.02503103	0.02503096

**Table 1:** Values of  $-\left|\theta'(1)\right|$  for  $Nt = Nb = a_1 = c_1 = d_1 = 0.1$ ,  $Pe = Le = 0.5$ ,  $Lb = 1$  with  $Re = 0.5$  for various expansion ratio ( $\alpha$ ) and thermal slip parameter ( $b_1$ ) values.

$b_1$	$-\left \theta'(1)\right $	$-\left \theta'(1)\right $	$-\left \theta'(1)\right $	$-\left \theta'(1)\right $	$-\left \theta'(1)\right $	$-\left \theta'(1)\right $
	Maple	Nakamura	Maple	Nakamura	Maple	Nakamura
	$\alpha=-0.5$	$\alpha=-0.5$	$\alpha=0$	$\alpha=0$	$\alpha=+0.5$	$\alpha=+0.5$
0.25	0.30960126	0.30960098	0.07392428	0.07392387	0.01684928	0.01684864
0.50	0.36323052	0.36323104	0.07665052	0.07665002	0.01698722	0.01698691
0.75	0.43746994	0.43746887	0.07957625	0.07957597	0.01712735	0.01712702
1.00	0.54493004	0.54493028	0.08272295	0.08272316	0.01726972	0.01726958

**Table 2:** Values of  $-\left|\theta'(1)\right|$  for  $Nt = Nb = a_1 = c_1 = d_1 = 0.1$ ,  $Pe = Le = 0.5$ ,  $Lb = 1$  with  $Re = 0.6$  for various expansion ratio ( $\alpha$ ) and thermal slip parameter ( $b_1$ ) values.

$c_1$	$-\left \phi(1)\right $	$-\left \phi(1)\right $	$-\left \phi(1)\right $	$-\left \phi(1)\right $	$-\left \phi(1)\right $	$-\left \phi(1)\right $
	Maple	Nakamura	Maple	Nakamura	Maple	Nakamura
	$\alpha=-0.5$	$\alpha=-0.5$	$\alpha=0$	$\alpha=0$	$\alpha=+0.5$	$\alpha=+0.5$
0.25	0.87883680	0.87883613	0.48948165	0.48948214	0.25131513	0.25131495
0.50	1.02368938	1.02368895	0.52535169	0.52535196	0.25985873	0.25985808
0.75	1.22567972	1.22567904	0.56689568	0.56689492	0.26900392	0.26900343
1.00	1.52688227	1.52688256	0.61557581	0.61557505	0.27881661	0.27881606

**Table 3:** Values of  $-\left|\phi(1)\right|$  for  $Nt = Nb = a_1 = b_1 = d_1 = 0.1$ ,  $Pe = Le = Lb = 0.5$  with  $Re = 0.9$  for various expansion ratio ( $\alpha$ ) and nano-particle mass slip parameter ( $c_1$ ) values.

$c_1$	$- \phi'(1) $	$- \phi'(1) $	$- \phi'(1) $	$- \phi'(1) $	$- \phi'(1) $	$- \phi'(1) $
	Maple	Nakamura	Maple	Nakamura	Maple	Nakamura
	$\alpha=-0.5$	$\alpha=-0.5$	$\alpha=0$	$\alpha=0$	$\alpha=+0.5$	$\alpha=+0.5$
0.25	0.77028858	0.77028903	0.41889688	0.41889712	0.21232448	0.21232463
0.50	0.87377120	0.87377201	0.44433169	0.44433221	0.21833443	0.21833491
0.75	1.00936233	1.00936197	0.47305578	0.47305614	0.22469470	0.22469405
1.00	1.19474231	1.19474274	0.50575154	0.50575093	0.23143684	0.23143702

**Table 4:** Values of  $-|\phi'(1)|$  for  $Nt = Nb = a_1 = b_1 = d_1 = 0.1$ ,  $Pe = Le = Lb = 0.5$  with  $Re = 1.0$  for various expansion ratio ( $\alpha$ ) and nano-particle mass slip parameter ( $c_1$ ) values.

**Tables 1 -4** show that temperature gradient i.e. upper wall heat transfer rate,  $|\theta'(1)|$ , decreases with increasing expansion parameter ratio and permeation Reynolds number.  $|\theta'(1)|$  however increases with increasing magnitude of thermal slip,  $b_1$ . Furthermore nano-particle solutal gradient i.e. nano-particle upper wall mass transfer rate  $|\phi'(1)|$  is found to consistently reduce with increasing  $\alpha$  and  $Re$ .  $|\phi'(1)|$  whereas it is enhanced significantly with increasing nano-particle mass slip,  $c_1$ .

## 5. COMPUTATIONAL RESULTS AND DISCUSSION

In this section Maple numerical graphical solutions are presented for the effects of several controlling parameters on the dimensionless velocity,  $f'(\eta)$ , temperature  $\theta(\eta)$ , nanoparticle volume fraction  $\phi(\eta)$  and motile micro-organism density function  $\chi(\eta)$ . We consider water-based bio-nanofluid for which  $Pr = 6.8$ . Maple solutions are presented in **Figs. 2-10**.

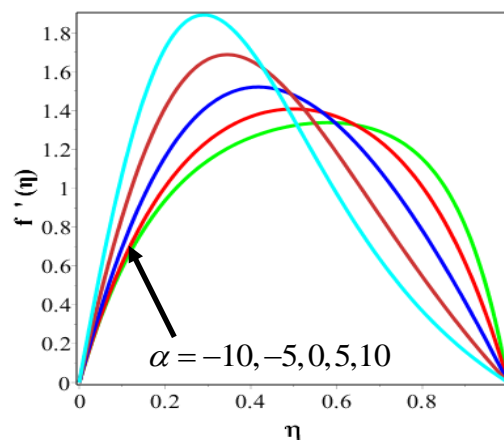


**Figure 2:** Effect of the expansion ratio parameter on velocity  $f'(\eta)$  with  $Re = 5$  (Maple RK45 solution) with  $Nt = Nb = a_1 = b_1 = c_1 = d_1 = 0.1$ ,  $Pe = Le = Lb = 0.5$ .



**Fig. 2** depicts the evolution in velocity  $f'(\eta)$  in the channel with variation in wall expansion ratio ( $\alpha$ ) with injection at the upper wall ( $Re = 5.0$ ). With negative  $\alpha$  (upper wall contracting) near the lower wall (static) and in the lower channel half space ( $0 \leq \eta \leq 0.5$ ) velocity is observed to be strongly reduced i.e. the flow is *decelerated*. Conversely with positive  $\alpha$  (upper wall expanding) near the lower wall (static) and in the lower channel half space ( $0 \leq \eta \leq 0.5$ ) velocity is observed to be strongly elevated i.e. the flow is accelerated. However in the *upper* channel half space ( $0.5 \leq \eta \leq 1.0$ ) the contrary behavior is computed i.e. the flow is decelerated with positive  $\alpha$  (upper wall expanding) whereas it is accelerated with negative  $\alpha$  (upper wall contracting). Evidently the greatest acceleration occurs closer to the lower plate for the expanding upper wall scenario since greater momentum transferred to the body of the fluid and this in conjunction with the injection at the upper wall (permeation Reynolds number,  $Re > 0$ ) aids flow development as far as into the lower channel half space. The geometry we have studied is employed in certain microbial fuel cell (MFC) designs. MFCs are biological fuel cells comprising a bio-electrochemical system which can be used to harness bacterial (micro-organism) propulsion to generate a current externally. The designs in which one wall is static and impervious and the other is stretchable have been shown to be potentially conducive to developing asymmetric flow distributions of micro-organisms which in turn can assist in increasing fuel cell efficiency. The extending/contracting nature of the upper wall in fact is used to simulate lipid layers in these fuel cells which possess natural elasticity. This allows them to adjust their state intelligently depending on the migration of micro-organisms towards the upper wall. This also works as a “smart” design feature in such fuel cells. Relevant works which elaborate on these structural wall features of next generation fuel cells include Du *et al.* [49] who explore applications of such features in environmental and bio-energy systems and Sun [50]. The presence of transpiration at the lower wall may further be used as a mechanism to simulate super-capacitive designs which utilize mass flux at one or more fuel cell walls to improve energy yield in more complex energy-harvesting bio-resource devices [51, 52]. In the present work we consider nanoscale-modified MFCs by exploring the *thermo-nano-bioconvection fluid dynamics* of such systems and do not dwell on efficiency (thermodynamic) aspects, although this constitutes a possible extension to the work, which is being considered presently and which it is envisaged may be explored by other researchers.

**Figs. 3(a)-(c)** display the variations in dimensionless temperature, nanoparticle volume fraction and motile micro-organism density function, respectively, for different values of wall expansion ratio ( $\alpha$ ) and permeation Reynolds number ( $Re$ ). Fig. 3a shows that for the expanding upper wall case ( $\alpha=0.5$ ), there is a weak *decrease* in temperatures throughout the channel span. Conversely for the contracting upper wall case, ( $\alpha = -0.5$ ) the temperature is weakly *increased*. The stationary upper wall case ( $\alpha=0$ ) is observed to fall between the expanding and contracting case profiles. With increasing permeation Reynolds number, temperature is significantly elevated throughout the channel width. This is attributable to the momentum boost in the flow associated with injected nanofluid via the upper wall. This assists thermal diffusion and energizes the channel flow which will elevate biofuel cell efficiency. Permeation Reynolds number embodies the relative significance of the inertia effect compared to the viscous effect. For  $Re = 1$  both inertial and viscous forces are of the same order of magnitude. However for  $Re = 3$ , inertial force significantly *exceeds* viscous forces and this in turn exacerbates the thermal diffusion in the nanofluid. In all cases, maximum temperatures are attained at the upper (dynamic) wall and profiles exhibit a monotonic ascent from the lower wall to converge smoothly at the upper wall. **Fig. 3b** demonstrates that nano-particle species concentration (volume fraction)  $\phi(\eta)$  is also enhanced with increasing Reynolds number from 1 to 3. The injection of nanofluid via the upper wall therefore serves to elevate concentration of suspended nano-particles in the channel and gradients of profiles are in fact sharper ascents than for the temperature field. However the influence of the expansion parameter is the reverse of that computed for the temperature field. For the expanding upper wall case ( $\alpha=0.5$ ), there is a substantial enhancement in nanoparticle volume fraction (concentration), whereas for the contracting upper wall case, ( $\alpha = -0.5$ ) the nanoparticle concentration is suppressed. The stationary upper wall case ( $\alpha=0$ ) again lies between these other two cases. For both the temperature and nano-particle concentration fields, the influence of Reynolds number and expansion parameter is sustained across the entire channel. **Fig. 3c** shows that the micro-organism density function, is increased with an expanding upper wall ( $\alpha=0.5$ ) whereas it is reduced with a contracting upper wall ( $\alpha = -0.5$ ), only in the region near the lower static wall; further from this zone there is a reversal in trends through the core flow one of the channel and for much of the channel upper half space. The pattern is then reversed again as we approach the upper wall. The peak micro-organism density values are localized closer to the lower static wall for  $Re = 3$ . They migrate further away for  $Re = 1$  and are in fact only increased in

magnitude for the solitary case of ( $\alpha=0.5$ ). For  $\alpha = -0.5, 0$  the magnitudes are markedly lower than for  $Re = 3$ ) although they are less asymmetrically distributed across the channel span. Generally however the expansion ratio and Reynolds number exert a significant influence on the magnitude of micro-organism density through the channel i.e. the concentration of micro-organisms demonstrates notable sensitivity to a contracting/expanding wall and also greater inertial forces (Reynolds number).

**Figure 4(a)-(d)** illustrate the response of effect of velocity (momentum) slip parameter  $a_1$  and wall expansion ratio ( $\alpha$ ) on dimensionless velocity, temperature, nanoparticle volume fraction and motile micro-organism density profiles, respectively. **Fig 4a** shows that velocity is weakly reduced near the lower wall of channel with positive  $\alpha$  i.e. slight deceleration is induced with an expanding upper wall, whereas the flow is weakly accelerated with negative  $\alpha$  i.e. contracting wall. Momentum slip is imposed only at the upper wall. It is absent from the lower wall, as is apparent from the boundary condition  $f'(1)=a_1f''(1)$  in eqn. (19). With an increase in  $a_1$ , velocity is accentuated in the lower channel half space whereas it is reduced in the upper channel half space, most prominently at the upper wall. Therefore lower momentum slip at the upper wall is observed to induce acceleration there whereas a strong deceleration is generated near the lower static wall. Greater momentum slip retards the fluid motion near and at the upper wall. Moreover, dragging of the fluid adjacent to the expanding wall is partially transmitted into the fluid partially which induces a deceleration. This result is in agreement with Raza *et al.* [36]. Fig. 4b reveals that dimensionless temperature decreases continuously as momentum slip is elevated i.e. with greater values of  $a_1$ . All profiles exhibit a monotonic ascent from the lower static wall to the upper wall. For an expanding wall ( $\alpha=+0.5$ ) temperature is decreased throughout the channel whereas for a contracting wall ( $\alpha=-0.5$ ) it is elevated. An expanding wall therefore cools the channel flow whereas a contracting wall heats it. Fig 4c shows that a weak increase in nano-particle volume fraction is caused with greater momentum slip and with a contracting wall ( $\alpha=-0.5$ ) whereas a marginal decrease is induced with an expanding wall ( $\alpha=+0.5$ ). Micro-organism density function is increased substantially near the lower static wall with an increase in momentum slip from  $a_1=1$  to  $a_1=10$ . However this behavior is reversed as we approach the central zone of the channel and progressively a marked reduction in micro-organism density function is observed as we approach the upper wall. The presence of an expanding upper wall has a similar effect to momentum slip i.e. it enhances micro-organism density function closer to the lower wall implying that the concentration of motile micro-organisms is intensified near the

lower wall. However towards the upper wall and indeed in the channel core flow region, the presence of an expanding wall is found to suppress micro-organism density function. The contracting wall case ( $\alpha = -0.5$ ) causes the opposite effect and depresses micro-organism density function near the lower static wall but *elevates* magnitudes towards the upper wall. The clustering and distribution of micro-organisms is therefore profoundly modified *throughout* the channel by the upper wall condition and also by momentum (hydrodynamic) slip *even though both conditions are only prescribed at the upper wall*.

**Figure 5** displays the influence of thermal slip parameter ( $b_1$ ) and expansion ratio ( $\alpha$ ) on dimensionless temperature,  $\theta(\eta)$ , in the channel. Thermal slip is also imposed solely at the upper wall, as embodied in the boundary condition  $\theta(1) = 1 + b_1 \theta'(1)$  in eqn. (19). Increasing thermal slip is found to *decrease* temperatures in the lower channel half space whereas it *elevates* temperatures in the upper channel half space i.e. in the region closer to the upper wall. Maximum temperature computed arises at the upper wall. With increasing thermal slip less heat is transmitted to the fluid in the lower channel half space whereas more heat is conveyed in the upper channel half space. The zone near and at the upper wall is therefore energized and heated. The influence of  $\alpha$  on temperature is primarily modelled via the term,  $Pr\alpha\eta\theta'$  in eqn. (16). The presence of an expanding wall ( $\alpha = +0.5$ ) decreases temperatures through the channel whereas a contracting wall manifests in a temperature increase.

**Figures 6(a)-(b)** depict the impact of mass slip parameter on dimensionless concentration  $\phi(\eta)$  and motile micro-organism density function,  $\chi(\eta)$  through the channel space. Fig. 6a shows that as with momentum and thermal slip, nano-particle mass slip is imposed only at the upper wall via the boundary condition  $\phi(1) = 1 + c_1 \phi'(1)$  in eqn. (19). Unlike the temperature response in fig. 5, nano-particle volume fraction is observed to be enhanced throughout the entire channel with increasing mass slip, as shown in fig. 6a. Peak values are achieved as expected at the upper wall. The diffusion of nano-particles is therefore assisted in the nanofluid with greater mass slip at the upper wall. Higher distributions of nanoparticles can therefore be encouraged everywhere in the channel with the prescription of mass slip at the upper wall, which has important implications for attaining better thermal performance throughout the entire channel, not merely in localized zones. The influence of  $\alpha$  on nano-particle concentration is analyzed via the term,  $PrLe\alpha\eta\phi'$  in eqn. (17). Confirming earlier

graphs, we observe that an *expanding* wall ( $\alpha=+0.5$ ) suppresses nano-particle volume fraction magnitudes whereas a *contracting* wall ( $\alpha=-0.5$ ) is responsible for enhancing them.

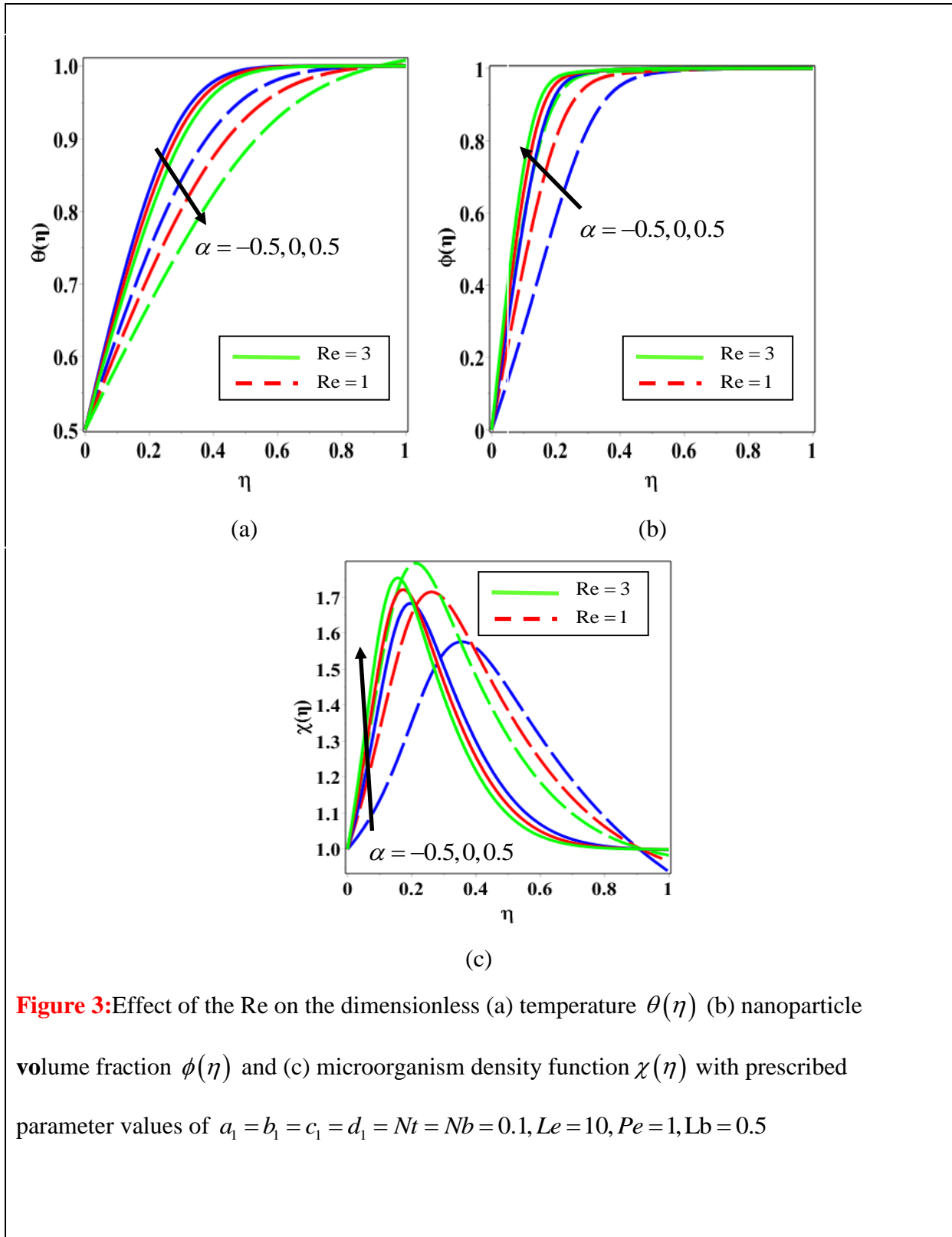
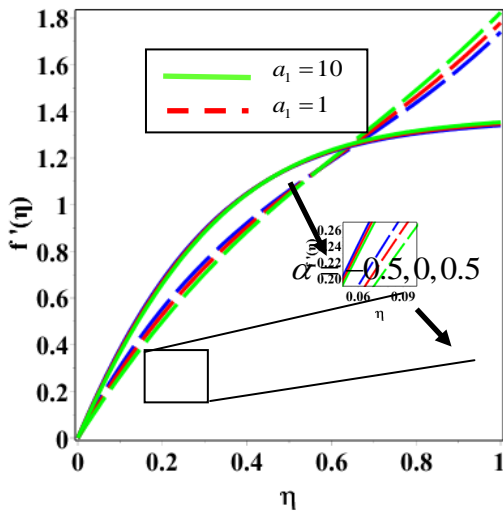
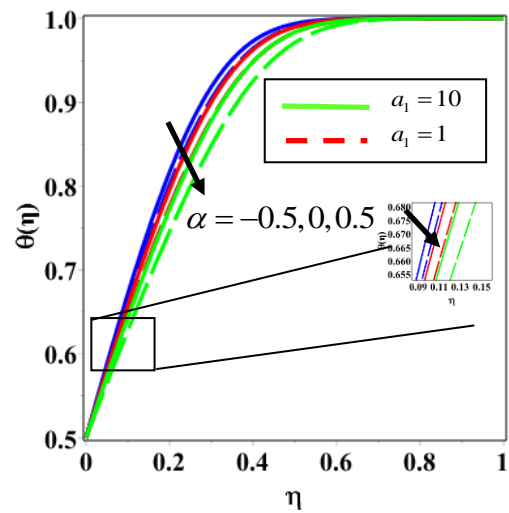


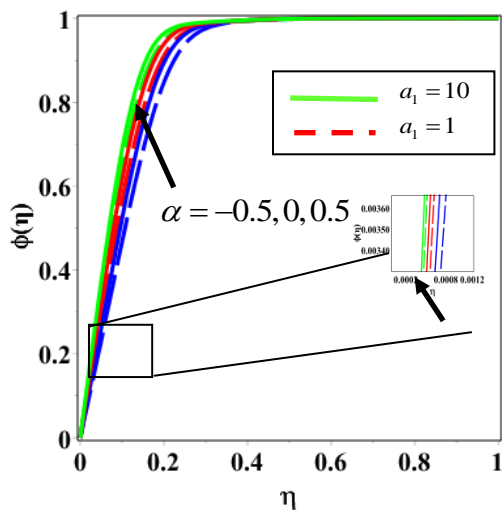
**Figure 3:** Effect of the Re on the dimensionless (a) temperature  $\theta(\eta)$  (b) nanoparticle volume fraction  $\phi(\eta)$  and (c) microorganism density function  $\chi(\eta)$  with prescribed parameter values of  $a_1 = b_1 = c_1 = d_1 = Nt = Nb = 0.1, Le = 10, Pe = 1, Lb = 0.5$



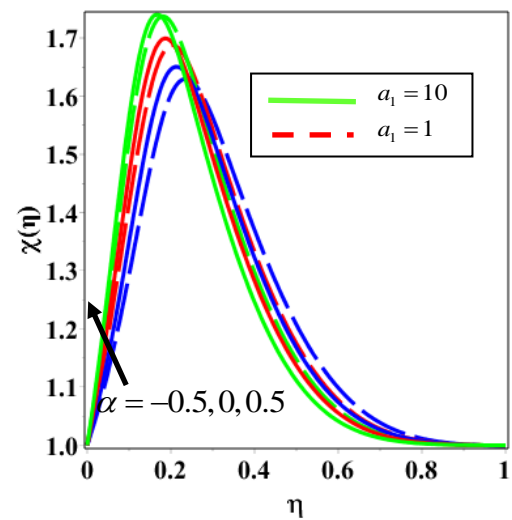
(a)



(b)



(c)



(d)

**Figure 4:** Effect of the velocity slip parameter  $a_1$  on the dimensionless (a) velocity  $f'(\eta)$  (b) temperature  $\theta(\eta)$  (c) nanoparticle volume fraction  $\phi(\eta)$  and (d) micro-organism density function  $\chi(\eta)$  with values  $b_1 = c_1 = d_1 = Nb = Nt = 0.1$ ,  $Le = 10$ ,  $Pe = 1$ ,  $Lb = 0.5$ ,  $Re = 5$ .

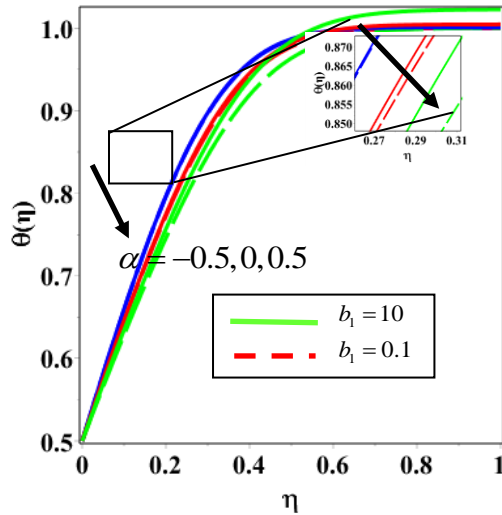


**Figure 5:** Effect of the thermal slip parameter  $b_1$  on the dimensionless temperature  $\theta(\eta)$  with parameter values of  $a_1 = b_1 = c_1 = d_1 = Nt = Nb = 0.1, Le = 10, Pe = 1, Lb = 0.5, Re = 2$ .

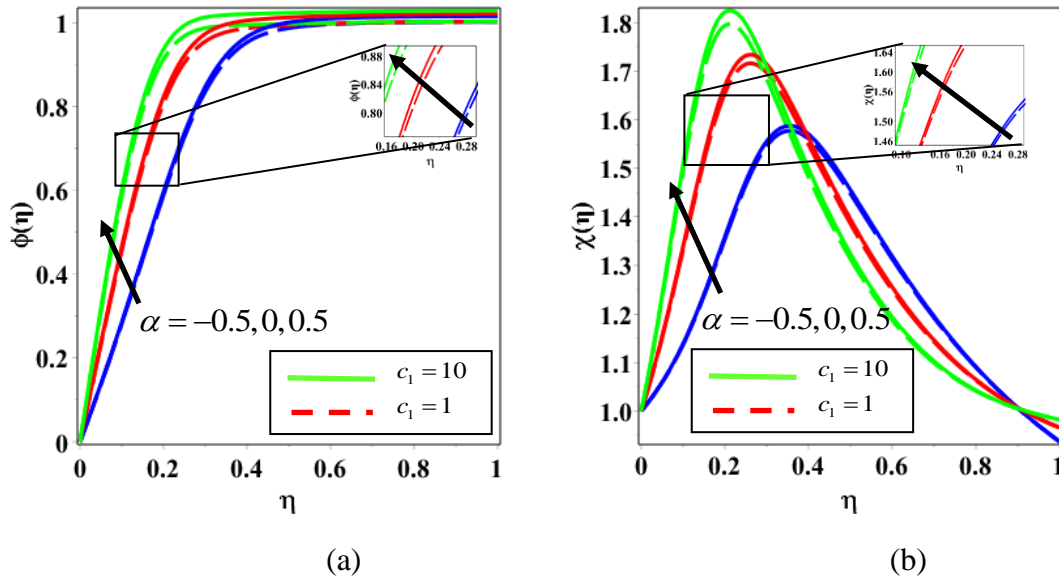


**Figure 6:** Effect of the mass slip parameter  $c_1$  on the dimensionless a) nanoparticle volume fraction  $\phi(\eta)$  and (b) microorganism density function  $\chi(\eta)$  with parameter values of  $a_1 = b_1 = d_1 = Nb = Nt = 0.1, Le = 10, Pe = 1, Lb = 0.5, Re = 1$ .

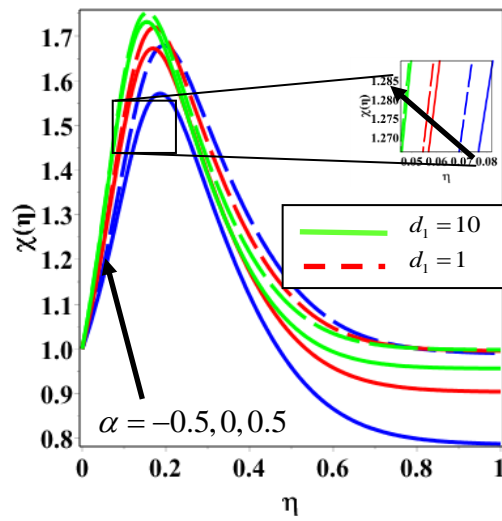
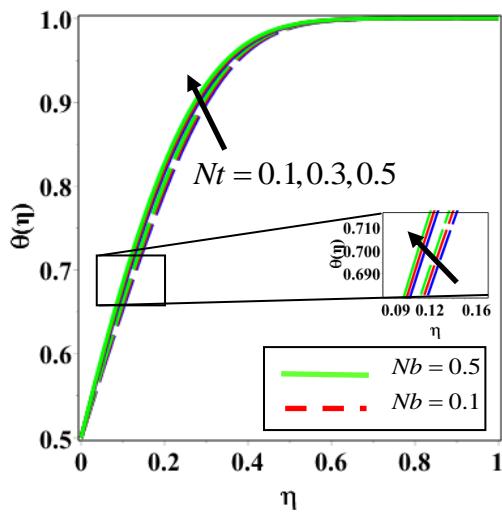
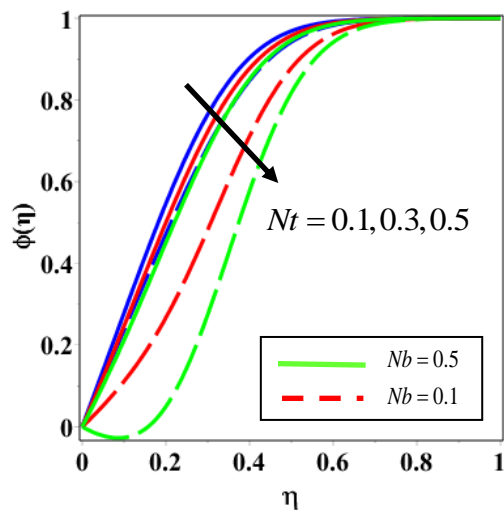


**Figure 7:** Effect of the micro-organism slip parameter  $d_1$  on the dimensionless micro-organism density  $\chi(\eta)$  with  $a_1 = b_1 = c_1 = Nb = Nt = 0.1, Le = 10, Pe = 1, Lb = 0.5, Re = 3$ .

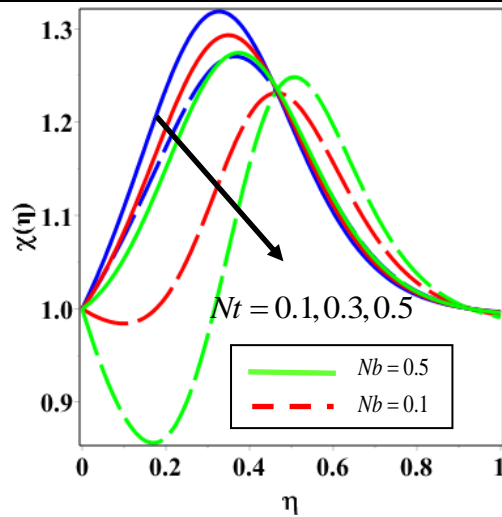


(a)



(b)





(c)

**Figure 8:** Effect of the thermophoresis parameter  $Nt$  and Brownian motion parameter  $Nb$  on the dimensionless (a) temperature  $\theta(\eta)$  (b) nanoparticle volume fraction  $\phi(\eta)$  and (c) microorganism density function  $\chi(\eta)$  with parameter values of  $a_l = b_l = c_l = d_l = 0.1, Le = 1, Pe = 1, Lb = 0.5, Re = 3, \alpha = -0.5$ .

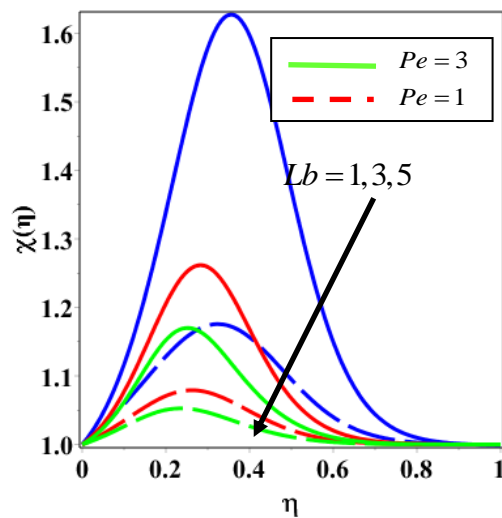


**Figure 9:** Effect of the bioconvection Péclet number  $Pe$  and bioconvection Lewis number  $Lb$  on the dimensionless micro-organism density function  $\chi(\eta)$  with  $a_l = b_l = c_l = d_l = Nb = Nt = 0.1, Le = 1, Re = 3, \alpha = -0.5$

Therefore combining mass slip and contracting behaviour at the upper wall, overall achieves the best performance and sustains the highest magnitudes in the channel for nano-particle volume fraction. Fig. 6b shows that nano-particle mass slip also exerts a beneficial effect on the motile micro-organism density function magnitudes. However the expansion ratio has the reverse effect to that on the nano-particle volume fraction field. An expanding wall ( $\alpha = +0.5$ ) strongly boosts the magnitudes of  $\chi(\eta)$  through the entire channel whereas a contracting wall results in a significant depression in  $\chi(\eta)$  values everywhere. The influence of  $\alpha$  on micro-organism density function is primarily simulated via the expansion ratio-micro-organism coupling term,  $LbPr\alpha\eta\chi'$  in eqn. (18). Also evident is the fact that the peak micro-organism density values migrate progressively from the lower static wall towards the central zone of the channel as the upper wall changes from an expanding one to a contracting one, with the stationary upper wall case intercalated between the other two cases. The distributions also become more symmetric across the channel span. Therefore although an expanding upper wall elevates substantially the micro-organism density magnitudes, these are confined to the lower channel half space i.e. they are skewed towards the lower wall. Conversely the contracting upper wall, although attaining lower magnitudes of micro-organism density, nevertheless generates a more *homogenous distribution* across the channel which may impact on microbial fuel cell efficiency. Irrespective of the value of mass slip or expansion ratio, micro-organism densities are generally minimized at the *upper* wall. Therefore fuel cell designers engaged in employing bioconvection in nanofluids are required to judiciously deploy upper wall boundary conditions and also nano-particle slip to optimize micro-organism replenishment and proliferation which impacts heavily on sustainable efficiency of such systems. Further elaboration is given in Croze *et al.* [53]. In fig. 6a we have considered the case  $Re = 1$  implying that inertial forces are equivalent to viscous forces in the channel. Further investigation, preferably experimental would shed greater light on the inter-play between these forces and the susceptibility of micro-organism concentration and also nano-particle diffusion to variation in the relative inertial and viscous effects.

**Figure 7** illustrates the impact of micro-organism slip parameter ( $d_1$ ) on dimensionless motile micro-organism density function,  $\chi(\eta)$  through the channel space. This slip factor is applied at the upper wall, in a similar fashion to thermal and nano-particle mass slip via the boundary condition  $\chi(1) = 1 + d_1 \chi'(1)$  in eqn. (19). A more uniform response is computed compared with the effect of nano-particle mass slip (which was studied earlier in fig. 6b). Increasing micro-organism slip substantially elevates the micro-organism density

function primarily in the vicinity of the lower wall. The maximum,  $\chi(\eta)$  magnitude arises therefore in the lowest region of the lower channel half space. However as we approach the lower central core region of the channel ( $0.2 \leq \eta \leq 0.3$ ) there is a switch in behavior and increasing micro-organism slip at the upper wall is observed to induce a marked decrease in  $\chi(\eta)$  magnitudes which is sustained throughout the upper channel half space.  $\chi(\eta)$  values progressively deplete until they attain a minimum at the upper wall. At the upper wall therefore micro-organism density function is a maximum for lowest micro-organism slip factor ( $d_1=1$ ). The presence of an expanding upper wall ( $\alpha = +0.5$ ) encourages motile micro-organism density enhancement near the lower wall whereas a contracting upper wall (i.e. expansion parameter  $\alpha = -0.5$ ) suppresses values. We further note that very low values of momentum, thermal and nano-particle mass slip ( $\ll 1$ ) are imposed to allow the dominant effect of micro-organism slip to be evaluated.

**Figure 8** illustrates the collective influence of nano-particle thermophoresis parameter ( $Nt$ ) and the Brownian motion parameter ( $Nb$ ) on the dimensionless temperature, nanoparticle volume fraction and motile micro-organism density function distributions across the channel. The contracting upper wall case is examined ( $\alpha = -0.5$ ). Increasing Brownian motion parameter physically correlates with *smaller nanoparticle diameters*, as elaborated in Rana *et al.* [54] and Akbar *et al.* [55]. Smaller values of  $Nb$  corresponding to larger nanoparticles, implies that surface area is reduced which in turn decreases thermal conduction heat transfer to the fluid. This coupled with macro-convection manifests in fig. 8a, in a non-trivial decrease in thermal energy imparted to the fluid and a concomitant fall in temperature,  $\theta(\eta)$ . The reverse effect is induced with larger values of  $Nb$  which correlate with smaller nano-particles and enhanced thermal conduction leading to higher temperatures. An increase in  $Nt$  also induces a rise in temperatures. Thermophoretic migration of nano-particles encourages thermal diffusion in the regime and energizes the flow. This elevates temperatures. Fig. 8b also shows that an elevation in nano-particle volume fraction,  $\phi(\eta)$ , accompanies an increase in Brownian motion parameter,  $Nb$ . In fact much greater enhancement is achieved compared with the temperature field. Increasing thermophoresis parameter,  $Nt$ , conversely suppresses the magnitudes of nano-particle volume fraction,  $\phi(\eta)$ . Nano-particle volume fraction is observed to ascend from zero values at the lower plate to maximum magnitudes at the upper wall, and all profiles approach this latter limit smoothly. Inspection of fig. 8c reveals that micro-organism density function profiles are distinctly different from the temperature and nano-particle concentration distributions. While increasing

$Nb$  values evidently promote diffusion of micro-organisms and achieve significant enhancement in their magnitudes, conversely increasing thermophoretic parameter,  $Nt$ , substantially depresses values. These trends are however restricted to the lower channel half space. In the upper channel half space on the other hand, increasing thermophoresis is found to elevate  $\chi(\eta)$  magnitudes whereas increasing Brownian motion parameter *increases*  $\chi(\eta)$  magnitudes. However peak values of micro-organism density function,  $\chi(\eta)$  are localized in the lower channel half space. The minimum value of  $\chi(\eta)$  is observed to arise in the lower channel half space at  $\eta \sim 0.2$ , for  $Nt = 0.5$  and  $Nb = 0.1$ .

**Figure 9** demonstrates the composite effects of bioconvection Lewis number and bioconvection Péclet number on the dimensionless micro-organism density function. The dimensionless micro-organism density magnitudes increase massively with in an increase  $Pe$  whereas they are reduced significantly with an increase in  $Lb$ . In the computations, standard Lewis number is prescribed as  $Le = 1$  which physically implies that thermal diffusivity of the nanofluid and species diffusivity of the nano-particles are the same.  $Pe$  i.e. bioconvection Péclet number embodies the ratio of advection rate of nano-particles to the diffusion rate.  $Pe < 10$  is more realistic for simulating actual transport phenomena in bioconvection nanofluid mechanics.  $Pe$  features only in the micro-organism density conservation eqn. (18) via the coupling terms  $-Pe(\phi' \chi' + \chi \phi'')$  which intimately connects the nano-particle concentration (volume fraction) and micro-organism fields. These terms evidently have a pronounced influence on the evolution of micro-organism density function in the channel. Bioconvection Lewis number,  $Lb$ , signifies the ratio of *dynamic viscosity of nanofluid* to the *species diffusivity of micro-organisms*, i.e.  $\nu/D_n$  arises solely in the micro-organism density conservation eqn. (18). It features in the velocity-micro-organism density coupling term,  $LbPrRe f\chi'$  and furthermore in the expansion ratio-micro-organism coupling term,  $LbPr\alpha\eta\chi'$ . The effect of  $Lb$  will therefore also be sustained in the momentum field i.e. eqn (28). For  $Lb < 1$  the micro-organism diffusion rate exceeds viscous diffusion rate and vice versa for  $Lb > 1$ . With increasing  $Lb$  values there is a strong *suppression* in the micro-organism density magnitudes, attributable to the decrease in micro-organism species diffusivity in the nanofluid (or an increase in viscosity).

## 6. CONCLUSIONS

A two-dimensional unsteady laminar model for bioconvection nanofluid flow in a channel with multiple upper wall slip effects and upper wall expansion/contraction has been studied.

The upper wall is porous whereas the lower wall is stationary and impermeable surface and therefore injection is present at the upper wall. The governing partial differential equations for momentum, energy, nano-particle species (volume fraction) and motile micro-organism density conservation are transformed into a set of ordinary differential equations (ODEs) using similarity variables. The resulting high order nonlinear ODEs are solved numerically using Runge-Kutta-Fehlberg integration scheme available in the RK45 shooting algorithm in Maple software. Validation of solutions is achieved with a Nakamura tridiagonal second order accurate finite difference scheme. Solutions are presented graphically and demonstrate the significant influence of bioconvection Lewis number, bioconvection Peclet, momentum slip, thermal slip, nano-particle mass slip, micro-organism slip, upper wall expansion ratio, permeation Reynolds number, Brownian motion and thermophoretic parameter on all the field variables. The principal deductions from the present investigation may be summarized thus:

- (i) Adding nanoparticles into base fluid containing suspended gyrotactic micro-organisms serves to increase the nano-particle and micro-organism mass transfer rates and achieves a stable mixture (suspension).
- (ii) Increasing bioconvection Lewis number suppresses dimensionless micro-organism density magnitudes whereas the reverse effect is induced with increasing bioconvection Peclet number.
- (iii) An increase in Brownian motion parameter elevates micro-organism density function magnitudes whereas increasing thermophoretic parameter reduces them, in the lower channel half space.
- (iv) An increase in Brownian motion parameter also enhances nano-particle volume fraction values, *whereas greater* thermophoresis parameter depresses values, throughout the channel span. Increasing micro-organism slip is found to enhance micro-organism density function mainly in the zone near the lower wall of the channel.
- (v) An upper expanding wall decelerates the flow near the lower wall of channel whereas a contracting wall weakly accelerates the flow.
- (vi) Increasing momentum slip accelerates the flow in the lower channel half space whereas it decelerates the flow in the upper channel half space, most prominently at the upper wall.
- (vii) Increasing nano-particle mass slip at the upper wall elevates motile micro-organism density function magnitudes.
- (viii) Greater thermal slip reduces temperatures in the lower channel half space whereas it *enhances* temperatures in the upper channel half space.

(ix) An expanding upper wall significantly elevates micro-organism density function magnitudes through the entire channel whereas a contracting wall induces the opposite effect.

The present simulations have been confined to Newtonian bioconvection nanofluids. Future studies will explore non-Newtonian models e.g. viscoelastic formulations [54], and will be communicated shortly. Furthermore nano-particle geometric effects also warrant more detailed analysis [56, 57] and these will also be explored. Additionally the current study has been restricted to gyrotactic micro-organisms i.e. where compensating torques generated by shear and gravity effects manifest in *gyro-taxis* which controls the orientation of up-swimming micro-organisms via rotary motions. However many other taxes are prevalent and can be exploited in microbial fuel cell design. These include *rheotaxis* (where the dominant response is to shear in the ambient flow. Certain bacterial swimmers contain magnetic particles (magnetosomes) and these cause a strong bias of the swimming motion along magnetic field lines and are known as magnetotaxis. Gravitaxis is a *gravitational-driven or acceleration-driven taxis* and for certain photosynthetic algae predominant propulsion is generally vertically upwards. Other significant taxes are *photo-taxis* and *chemo-taxis* in which the dominant effect is a swimming towards more intense light and chemical gradients, respectively. All these taxes are in fact relevant to microbial fuel cell (MFC) design and in fact combinations may also be exploited. To simulate these taxes the hydrodynamic models must be modified to emphasize the particular taxis. This involves detailed micro-hydrodynamic analysis and modifications in hydrodynamic torque formulation. The direction in which a micro-organism swims, is defined at any instant by the balance of viscous and external torques on the cell. These external torques will be gravitational for gyrotaxis and will be modified for other external taxes e.g. phototaxis or chemo-taxis. This allows the model to be specific for a particular type of directional swimming behavior (light, oxygen concentration, etc.). Relevant photo-tactic and chemo-tactic models have been communicated in this regard by Ghorai and Hill [58] and Yanaoka *et al.* [59] and are currently being explored.

#### **ACKNOWLEDGEMENTS:**

The authors acknowledge financial support from Universiti Sains Malaysia, RU Grant 1001/PMATHS/81125. The authors are extremely grateful to both Reviewers for their excellent and informative comments which have certainly served to clarify and improve the present work. O. Anwar Bég expresses his deepest gratitude to Tazzy Bég.

## REFERENCES

- [1] Hedayati F and Domairry G., Nanoparticle migration effects on fully developed forced convection of TiO<sub>2</sub> – water nanofluid in a parallel plate microchannel, *Particuology* **24** 96–107.
- [2] Wu L., Mass transfer induced slip effect on viscous gas flows above a shrinking / stretching sheet *Int. J. Heat Mass Transf.* **93** 17–22 (2016).
- [3] Mosayebidorcheh S., Analytical investigation of the micropolar flow through a porous channel with changing walls *J. Mol. Liq.* **196** 113–9 (2014).
- [4] Odelu O. and Naresh Kumar N., Slip-flow and heat transfer of chemically reacting micropolar fluid through expanding or contracting walls with Hall and ion slip currents *Ain Shams Eng. J.* (2015). DOI:10.1016/J.ASEJ.2015.09.011
- [5] Adesanya S O, Free convective flow of heat generating fluid through a porous vertical channel with velocity slip and temperature jump *Ain Shams Eng. J.* 1045–52 (2014).
- [6] Uchida S and Aoki H., Unsteady flows in a semi-infinite contracting or expanding pipe *J. Fluid Mech.* **82** 371–87 (1977).
- [7] N.M. Bujurke, V.S. Madalli, B.G. Mulimani, Long series analysis of laminar flow through parallel and uniformly porous walls of different permeability, *Computer Methods in Applied Mechanics and Engineering*, 160, 39-56 (1998).
- [8] M.Goto and S. Uchida, Unsteady flows in a semi-infinite expanding pipe with injection through wall, *J. Japan Society for Aeronautical and Space Sciences*, 33, 14-27 (1990).
- [9] Hatami M, Sheikholeslami M and Ganji D D., Nanofluid flow and heat transfer in an asymmetric porous channel with expanding or contracting wall, *J. Mol. Liq.* **195** 230–9 (2014).
- [10] Boutros Y Z, Abd-el-Malek M B, Badran N A and Hassan H S., Lie-group method for unsteady flows in a semi-infinite expanding or contracting pipe with injection or suction through a porous wall *J. Comput. Appl. Math.* **197** 465–94 (2006).
- [11] Xinhui S, Liancun Z, Xinxin Z and Jianhong Y, Homotopy analysis method for the heat transfer in a asymmetric porous channel with an expanding or contracting wall *Appl. Math. Model.* **35** 4321–4329 (2011).
- [12] Si X, Zheng L, Zhang X, Li M, Yang J and Chao Y., Multiple solutions for the laminar flow in a porous pipe with suction at slowly expanding or contracting wall *Appl. Math. Comput.* **218** 3515–21 (2011).
- [13] Ahmed N, Mohyud-Din S T and Hassan S M Flow and heat transfer of nanofluid in an asymmetric channel with expanding and contracting walls suspended by carbon nanotubes: A numerical investigation *Aerosp. Sci. Technol.* **48** 53–60 (2016).
- [14] Darvishi M T, Khani F, Awad F G, Khidir A A and Sibanda P., Numerical investigation of the flow of a micropolar fluid through a porous channel with expanding or contracting walls *Propuls. Power Res.* **3** 133–142 (2014).

- [15] S.U. Choi, Enhancing thermal conductivity of fluids with nanoparticles, *Development and Applications of Non-Newtonian Flow*, FED-Vol. 231/MD-Vol. 66, ASME, 99–105 (1995).
- [16] J.A. Eastman, S.R. Phillpot, S.U.S. Choi, P. Keblinski, Thermal transport in nanofluids, *Ann. Rev. Mater. Res.* 34, 219-146 (2004).
- [17] Khairul M A, Shah K, Doroodchi E, Azizian R and Moghtaderi B., Effects of surfactant on stability and thermo-physical properties of metal oxide nanofluids *Int. J. Heat Mass Transf.* **98** 778–87 (2016).
- [18] O. Anwar Bég and D. Tripathi, Peristaltic pumping of nanofluids, *Chapter 3, pages 69-96, Modeling and Simulation Methods and Applications, Eds (S. K. Basu, N. Kumar), Springer, Berlin, Germany* (2014).
- [19] Kakaç S and Pramuanjaroenkij A., Review of convective heat transfer enhancement with nanofluids *Int. J. Heat Mass Transf.* **52** 3187–96 (2009).
- [20] Hamad M A A and Ferdows M., Similarity solution of boundary layer stagnation-point flow towards a heated porous stretching sheet saturated with a nanofluid with heat absorption / generation and suction / blowing : A Lie group analysis *Commun. Nonlinear Sci. Numer. Simul.* **17** 132–40 (2012).
- [21] Pedley T J, Hill N. and Kessler J. O. , The growth of bioconvection patterns in a uniform suspension of gyrotactic micro-organisms. *J. Fluid Mech.* **195** 223–37 (1988).
- [22] Uddin M.J., Kabir M N and O. Anwar Bég, Computational investigation of Stefan blowing and multiple-slip effects on buoyancy-driven bioconvection nanofluid flow with microorganisms, *International Journal of Heat and Mass Transfer.* **95** 116–30 (2016).
- [23] A. Raees, H. Xu, Q. sun and I. Pop, Mixed convection in gravity-driven nano-liquid film containing both nanoparticles and gyrotactic microorganisms, *Applied Mathematics and Mechanics*, 36, 163-178 (2015).
- [24] Raees A, Xu H and Liao S., Unsteady mixed nano-bioconvection flow in a horizontal channel with its upper plate expanding or contracting, *Int. J. Heat and Mass Transfer.* **86** 174–82 (2015).
- [25] Md Faisal Md Basir, M.J. Uddin, A. I. Md. Ismail and O. Anwar Bég, Unsteady bio-nanofluid slip flow over a stretching cylinder with bioconvection Schmidt and Péclet number effects, *AIP Advances*, **6**, 055316-1 - 055316-15 (2016).
- [26] J. Buongiorno Convective transport in nanofluids, *ASME J. Heat Transfer*, 128, 240–250 (2006).
- [27] A. Malvandi, S.A. Moshizi, Elias Ghadam Soltani, D.D. Ganji, Modified Buongiorno's model for fully developed mixed convection flow of nanofluids in a vertical annular pipe, *Computers & Fluids*, 89, 124–132 (2014).



- [28] Hang Xu, Tao Fan, Ioan Pop, Analysis of mixed convection flow of a nanofluid in a vertical channel with the Buongiorno mathematical model, *International Communications in Heat and Mass Transfer*, 44, 15–22 (2013).
- [29] M. A. Sheremet, Ioan Pop, Free convection in a triangular cavity filled with a porous medium saturated by a nanofluid: Buongiorno's mathematical model", *International Journal of Numerical Methods for Heat & Fluid Flow*, 25, 1138 – 1161 (2015).
- [30] N. S. Akbar, D. Tripathi, Z.Khan and O. Anwar Bég, A numerical study of magnetohydrodynamic transport of nanofluids from a vertical stretching sheet with exponential temperature-dependent viscosity and buoyancy effects, *Chemical Physics Letters*, 661, 20-30 (2016).
- [31] M.J. Uddin, O. Anwar Bég and A.I. Ismail, Radiative-convective nanofluid flow past a stretching/shrinking sheet with slip effects, *AIAA J. Thermophysics Heat Transfer*, 29, 3, 513-523 (2015).
- [32] M. J. Uddin, W.A. Khan, A.I.Md. Ismail, O. Anwar Bég, Computational study of three-dimensional stagnation point (Buongiorno) nanofluid bio-convection flow on a moving surface with anisotropic slip and thermal jump effects, *ASME J. Heat Transfer (USA)* (2016). DOI: 10.1115/1.4033581 (8 pages).
- [33] Kuznetsov A V. and Nield D. A., The Cheng-Minkowycz problem for natural convective boundary layer flow in a porous medium saturated by a nanofluid: A revised model *Int. J. Heat Mass Transf.*, 65, 682–5 (2013).
- [34] Dauenhauer E C and Majdalani J., Exact self-similarity solution of the Navier-Stokes equations for a porous channel with orthogonally moving walls, *Phys. Fluids* **15** 1485–95 (2003).
- [35] Cao L, Si X and Zheng L., The flow of a micropolar fluid through a porous expanding channel: A Lie group analysis *Appl. Math. Comput.* **270** 242–50 (2015).
- [36] Raza J, Rohni A M, Omar Z and Awais M., Heat and mass transfer analysis of MHD nanofluid flow in a rotating channel with slip effects *J. Mol. Liq.* **219** 703–8 (2016).
- [37] Pedley, T. J., Kessler, J. O. 1990. A new continuum model for suspensions of gyrotactic micro-organisms. *J. Fluid Mech.* 212: 155-82.
- [38] Hart, A., Edwards, C 1987. Buoyant density fluctuations during the cell cycle of *Bacillus subtilis*. *Arch. Microbiol.* 147: 68-72.
- [39] Md. Jashim Uddin, O. Anwar Bég and Ahmad Izani Md. Ismail, Mathematical modelling of radiative hydromagnetic thermo-solutal nanofluid convection slip flow in saturated porous media, *Math. Prob. Engineering*, **2014**, Article ID 179172, 11 pages (2014).
- [40] O. Anwar Bég, M. J. Uddin and W.A. Khan, Bioconvective non-Newtonian nanofluid transport in porous media containing micro-organisms in a moving free stream, *J. Mechanics Medicine Biology*, **15**, 1550071.1-1550071.20 (2015).
-

- [41] O. Anwar Bég and O.D. Makinde, Viscoelastic flow and species transfer in a Darcian high-permeability channel, *Petroleum Science and Engineering*, **76**, 93–99 (2011).
- [42] Nakamura, S., Iterative finite difference schemes for similar and non-similar boundary layer equations, *Adv. Eng. Software*, **21**, 123–130 (1994).
- [43] Bég, O. Anwar, NANONAK- A finite difference code for nanofluid convection problems of the boundary layer type, *Technical Report, NANO-C/5-1, 124pp, Gort Engovation, Bradford, England and Narvik, Norway, UK, August* (2013).
- [44] Bég, O. Anwar, J. Zueco, M. Norouzi, M. Davoodi, A. A. Joneidi, Assma F. Elsayed, Network and Nakamura tridiagonal computational simulation of electrically-conducting biopolymer micro-morphic transport phenomena, *Computers in Biology and Medicine*, **44**, 44–56 (2014).
- [45] Bég, O. Anwar, T. A. Bég, H. S. Takhar, A. Raptis, Mathematical and numerical modeling of non-Newtonian thermo-hydrodynamic flow in non-Darcy porous media, *Int. J. Fluid Mech. Res.*, **31**, 1–12 (2004).
- [46] Gorla, R.S.R. and S. Nakamura, Combined convection from a rotating cone to micropolar fluids, *Math. Modelling Sci. Comput.*, **2**, 1249–1254 (1993).
- [47] Nakamura, S., *Applied Numerical Methods and Software*, Prentice-Hall New Jersey, USA (1995).
- [48] Bég, O. Anwar, Numerical methods for multi-physical magnetohydrodynamics, Chapter 1, pp. 1-112, *New Developments in Hydrodynamics Research*, M. J. Ibragimov and M. A. Anisimov, Eds., Nova Science, New York, September (2012).
- [49] Z. Du, H. Li, and T. Gu, A state of the art review on microbial fuel cells: A promising technology for wastewater treatment and bioenergy, *Biotechnology Advances*, **25**, 464-482 (2007).
- [50] Y. Sun, Electricity generation and microbial community changes in microbial fuel cells packed with different anodic materials, *Bioresource Technology*, **10**, 10886-10891 (2011).
- [51] H. Wang, J-D. Park and Z. J. Ren, Practical energy harvesting for microbial fuel cells: a review, *Environ. Sci. Technol.*, **49** (6), 3267–3277 (2015).
- [52] J. Houghton, C. Santoro, F. Soavi, A. Serov, I. Ieropoulos, C. Arbizzani, P. Atanassov, Supercapacitive microbial fuel cell: Characterization and analysis for improved charge storage/delivery performance, *Bioresource Technology*, **218**, 552-560 (2016).
- [53] O.A. Croze, E. Ashraf and M. Bees, Sheared bioconvection in a horizontal tube, *Physical Biology*, **7**(4):046001 (2010).
- [54] P. Rana, R. Bhargava, O. Anwar Bég and A. Kadir, Finite element analysis of viscoelastic nanofluid flow with energy dissipation and internal heat source/sink effects, *Int. J. Applied Computational Mathematics*, 1-27 (2016). DOI 10.1007/s40819-016-0184-5.
-

- [55] N. S. Akbar, O. Anwar Bég, Z. H. Khan, Magneto-nanofluid flow with heat transfer past a stretching surface for the new heat flux model using numerical approach, *Int. J. Num. Meth. Heat Fluid Flow* (2016). ***In press***
- [56] N. S. Akbar, D. Tripathi and O. Anwar Bég, Modelling nanoparticle geometry effects on peristaltic pumping of medical magnetohydrodynamic nanofluids with heat transfer, *J. Mechanics in Medicine and Biology*, 16 (2) 1650088.1-1650088.20. DOI: 10.1142/S0219519416500883 (2015).
- [57] A. Askounis *et al.*, Effect of particle geometry on triple line motion of nano-fluid drops and deposit nano-structuring, *Advances in Colloid and Interface Science*, 222, 44–57 (2015).
- [58] S. Ghorai and N.A. Hill, Penetrative phototactic bioconvection, *Phys. Fluids*, 17, 074101 (2005).
- [59] H. Yanaoka, T. Inamura, K. Suzuki, Numerical analysis of bioconvection generated by chemotactic bacteria, *Japan Soc. Mech. Eng. J. Fluid Science and Technology*, 4, 536-545 (2009).
-